

Probe Design for the Eddy Current Inspection of Cooling Tubes in the Blanket of a Fusion DEMO Reactor^{*})

Mizuki KAKO¹⁾, Takuma TOMIZAWA¹⁾, Jiu hao GE^{1,2)}, Takashi NOZAWA³⁾ and Noritaka YUSA¹⁾

¹⁾Graduate School of Engineering, Tohoku University, 6-6-01-2 Aramaki Aza Aoba, Sendai 980-8579, Japan

²⁾Nondestructive Detection and Monitoring Technology for High Speed Transportation Facilities, Nanjing University of Aeronautics and Astronautics, Nanjing, Jiangsu, 211106, China

³⁾National Institutes for Quantum Science and Technology, 2-166 Obuchi Omotedate, Rokkasho-mura 039-3212, Japan

(Received 20 December 2021 / Accepted 13 September 2022)

This study investigated the applicability of eddy current testing (ECT) to the non-destructive inspection of cooling tubes in the blanket of a fusion DEMO reactor. Pipes made of F82H steel with inner and outer diameters of 9.0 and 11.0 mm, respectively, were prepared, and slits imitating cracks were fabricated on the pipe surfaces. ECT was performed using a differential type bobbin probe having one exciting and two detecting coils designed in this study. The results of the inspections and subsequent three-dimensional finite element simulations revealed that a bobbin probe is effective in detecting cracks appearing on the inner surface of a pipe. Moreover, the detectability does not deteriorate significantly when cracks oriented in the circumferential directions are targeted, unlike in the case of ECT of the heat exchanger tubes of the steam generators of the pressurized water reactors. This indicates that a probe with a more complicated structure, such as a plus-point probe, would be unnecessary to detect flaws on the inner surface of a pipe. In contrast, the ECT signals from a non-penetrating slit on the outer surface were buried in noise even though the slit was as deep as 0.9 mm.

© 2022 The Japan Society of Plasma Science and Nuclear Fusion Research

Keywords: ECT, F82H, blanket, prototype reactor, cooling tube, ferromagnetic, bobbin probe

DOI: 10.1585/pfr.17.2405102

1. Introduction

A fusion DEMO reactor is planned to be built in Japan as the next step to ITER to demonstrate the net production of electric power from nuclear fusion [1, 2]. One of the most important components for this purpose is the blanket that covers the interior surfaces of the vacuum vessel and transforms the kinetic energy of the neutrons into heat energy. Many cooling tubes are situated in the blanket to transfer the produced heat [3]. The failure of these tubes leads to the leakage of the coolant, which is a severe problem in reactor operation. Therefore, the integrity of the cooling tubes must be ensured using a proper non-destructive inspection method.

The most promising method for the non-destructive inspection of the cooling tubes is eddy current testing (ECT) because of its suitability for the rapid inspection of many components with a simple shape. ECT can operate automatically and remotely, which is advantageous for inspecting many components in a radiation environment. Since the early beginning of nuclear power, ECT has been applied to the non-destructive inspection of the heat exchanger tubes of the steam generators of pressurized water reactors (PWR-SGs) [4–6]. Whereas these imply that ECT

is effective for the inspection of the cooling tubes, the applicability of ECT to the inspection of the tubes has not been investigated so far. This is because a fusion DEMO reactor is still at the design stage, and thus, the detailed design of the cooling tubes, as well as that of the blanket, has not been decided yet. However, whether a proper non-destructive inspection is available is a critical issue in designing components whose failure must be avoided. Thus, for the further practical design of a blanket for the fusion DEMO reactor, evaluating the applicability of ECT to the cooling tubes is critical.

Among the several possible designs of the cooling tubes, their most significant difference from the heat exchanger tubes of the PWR-SGs from the viewpoint of ECT is that they are made of F82H reduced activation ferritic/martensitic steel [7–9]. This is because ECT becomes insensitive when it is applied to magnetic materials in general [10]. An earlier study by the authors evaluated the magnetic property of F82H steel and confirmed that the magnetic property of F82H steel is regarded as linear under weak electromagnetic fields commonly used in ECT [11]. A subsequent study evaluated the applicability of ECT to the detection of slits on F82H plates using several different types of probes [12]. The study revealed that the noise arising from the magnetism of F82H steel was much lower than that from austenitic stainless steel welds [13], and ob-

author's e-mail: mizuki.kako.r7@dc.tohoku.ac.jp

^{*}) This article is based on the presentation at the 30th International Toki Conference on Plasma and Fusion Research (ITC30).

tained clear signals from a slit as shallow as 0.1 mm even when an absolute type pancake probe was used. In addition, the study confirmed clear signals from the slit when induced eddy currents flow parallel to the slit due to the effect of magnetic flux leakage [14]. These findings imply that a bobbin probe, which induces eddy currents only in the circumferential direction, would be able to detect a flaw appearing on the tube regardless of the orientation of the flaw, unlike when ECT is applied to the heat exchanger tubes of the PWR-SGs. Generally, the bobbin probe has low detectability of circumferential slits in the case of inspection of heat exchanger tubes of the PWR-SGs, and a complex design probe was used for inspection. In contrast, a bobbin probe is the simplest internal probe, and it is preferable especially when targeting pipes with a small diameter, such as the cooling tubes of a blanket.

Hence, this study investigated the applicability of ECT using a bobbin probe to the non-destructive inspection of the cooling tubes of a blanket. Because the specific design of a cooling tube is still undecided, this study used straight F82H pipes with an inner diameter and thickness of 9.0 and 1.0 mm, respectively, to simulate one of the recent designs [3]. Cracks appearing on the tube wall were targeted because they are usually one of the most harmful defects and are difficult to detect. Through experimental verifications and three-dimensional finite element simulations, the applicability of ECT to the non-destructive inspection of a cooling tube with a different design was discussed.

2. Materials and Methods

2.1 Experiment

Figure 1 illustrates the bobbin probe designed in this study. The probe consisted of one exciting coil and two detecting coils and outputs the difference between the induced voltages of the two detecting coils as the signals. The number of turns of the three coils was 115. The outer diameter of the probe is approximately half of that used in PWR-SGs [15]. Whereas this study made another probe with the same dimension but with permanent magnets to reduce magnetic noise from F82H pipes, experimental verification did not confirm the improvement of the signal-to-noise ratio. Thus, this paper presents only results obtained using the probe shown in the figure.

The probe was connected to a commercial eddy current instrument, aect-2000N (aswan ect Co., Ltd., Osaka, Japan). The exciting frequency, exciting current, and magnetomotive force were 100 kHz, 11.8 mA, and 1.36 A, respectively. A centering device made of resin was attached to the probe to place it in the center of the pipe, and the probe was controlled using an XY stage. The scan length was 80 mm, and the scan pitch was 0.1 mm. The measurement was performed five times with the same conditions to confirm the reproducibility.

To evaluate the detectability of the probe, two groups of pipes were prepared. Group 1 contained 15 short

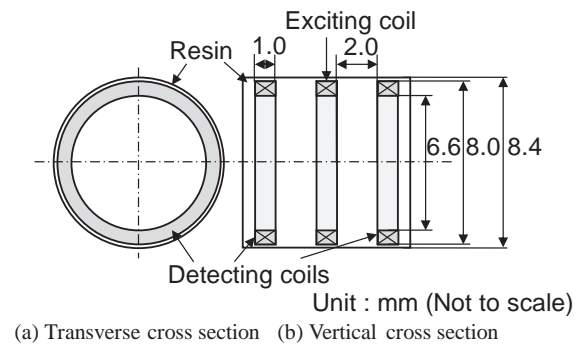


Fig. 1 The design of the bobbin probe.

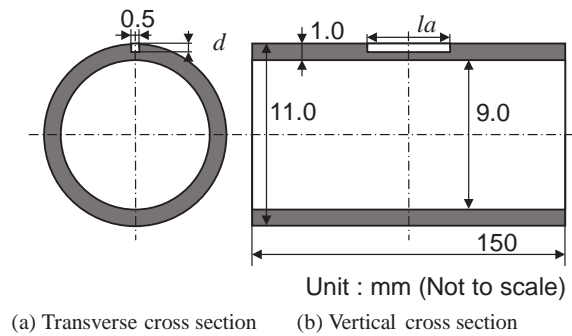


Fig. 2 Specimen having the axial slit.

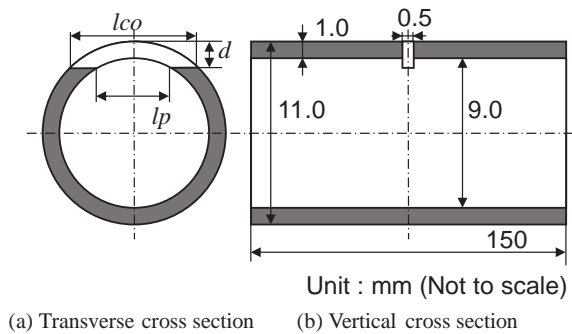


Fig. 3 Specimen having the circumferential slit.

straight pipes made of F82H steel. The outer diameter, inner diameter, thickness, and length of the pipes were 11.0, 9.0, 1.0, and 150 mm, respectively. The axial and circumferential slits imitating the cracks, as shown in Figs. 2 and 3, were fabricated in the 12 pipes of them using the electro-discharge machining. The parameters of the slits are summarized in Tables 1 and 2. All the slits were fabricated on the outer surface of the pipe because fabricating slits on the inner surface was difficult. Three F82H short pipes without slits, which were termed as F82H pipe 1, 2, and 3, were measured to evaluate magnetic noise. As a substitute, the detectability of the probe against non-penetrating slits on the inner surface was evaluated using numerical simulations. The pipes were demagnetized using a portable demagnetizer HC-31 (HOZAN TOOL IND. Co., Ltd., Osaka, Japan), whereas the earlier study confirmed that the

Table 1 The parameters of the designed axial slits.

Depth, d [mm]	Axial length, la [mm]
0.5	5
0.7	5
0.9	5
1.0	2
1.0	5
1.0	10

Table 2 The parameters of the designed circumferential slits.

Depth, d [mm]	Circumferential length of outer surface, lco [mm]	Penetration length, lp [mm]
0.5	4.6	-
0.7	5.4	-
0.9	6.0	-
1.1	6.6	1.9
1.5	7.5	4.1
3.0	9.8	7.5

demagnetization using the demagnetizer did not largely reduce the magnetic noise of the F82H steel.

Group 2 contained aluminum alloy (A6063) pipes having the same dimensions and slits as those of Group 1 which were used to indicate the effect of F82H's magnetic property on signals. Two aluminum alloy pipes without slits, named Al pipe 1 and 2, were prepared to evaluate noise.

2.2 Numerical simulation

Numerical simulations were conducted to evaluate the detectability of the probe against inner surface slits on the F82H pipes and the effect of the exciting frequency on the signals. The commercial 3D finite element method software, COMSOL Multiphysics®ver. 5.5 was employed with its ACDC module. The governing equation in the software is as follows [16]:

$$(j\omega\sigma - \omega^2\epsilon_0\epsilon_r)\mathbf{A} + \nabla \times \frac{1}{\mu_0\mu_r}(\nabla \times \mathbf{A}) = \mathbf{J}_e, \quad (1)$$

where ω , σ , ϵ_0 , ϵ_r , μ_0 , μ_r , \mathbf{A} , and \mathbf{J}_e are angular frequency, conductivity, vacuum permittivity, relative permittivity, vacuum permeability, relative permeability, magnetic vector potential, and exciting current density, respectively.

The material properties are summarized in Table 3 [11]. The exciting current density of the exciting coil was set to 1.429 A/mm², whereas the linearity of the governing equation indicates that it is not essential in this study. The amplitude and phase of the signal caused by the axial penetrated slit with a length of 10 mm were used to calibrate the numerical signals to enable quantitative comparison with those obtained in the experiments. Specifically, the numerical signal caused by the axial penetrated slit with a length

Table 3 Material properties.

Material	Conductivity σ [S/m]	Relative permeability μ_r [-]	Relative permittivity ϵ_r [-]
F82H [11]	2.2×10^6	44	1
Air	10	1	1

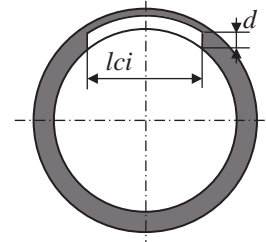


Fig. 4 Inner surface circumferential slit used in the numerical simulation.

of 10 mm was amplified and rotated on a 2D plane so that its amplitude and phase match those of the experimental signals caused by the slit of the same dimension. Subsequently, all the numerical signals were amplified and rotated using the same amplification and rotation angle. This is a general procedure in quantitatively analyzing numerical signals to compensate for the effects of the impedance of the probe and circuit that are usually unknown. The exciting frequencies used were 1, 3, 10, and 100 kHz.

The slits and pipes were modeled using the parameters as those of the specimens used in the experiment. Additional non-penetrating inner surface slits were prepared. The circumferential slits were modeled with an arc-shaped depth profile, as shown in Fig. 4, to avoid the finite elements having acute angles. In Fig. 4, lci represents the circumferential length of an inner surface slit. The pipe, slit, and coil regions were divided into triangular prism elements, and the air region was divided into tetrahedron elements. The maximum element size of the pipe near the slit was 0.16 mm.

3. Results

3.1 Evaluation of detectability by experiment

3.1.1 Detectability against the penetrated slits

Figures 5 and 6 present the trajectories of the ECT signals from the F82H pipes without slits and with the penetrated slits, respectively. The X- and Y-components of the figures mean the in-phase and quadrature components of the measured signals. Figure 5 shows three signals from the pipes without slits having different amplitudes. Signals from F82H pipes without slits 1 and 2 are much larger than that from F82H pipe 3. It is probable that the crystal grains of F82H steel had an orientation when processed into the

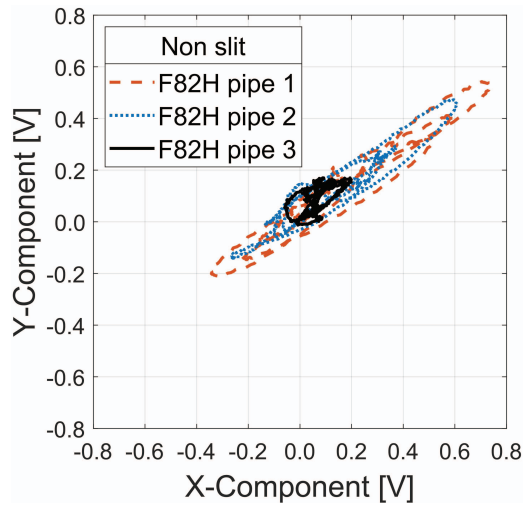


Fig. 5 The trajectories of the ECT signals from the F82H pipes without slits.

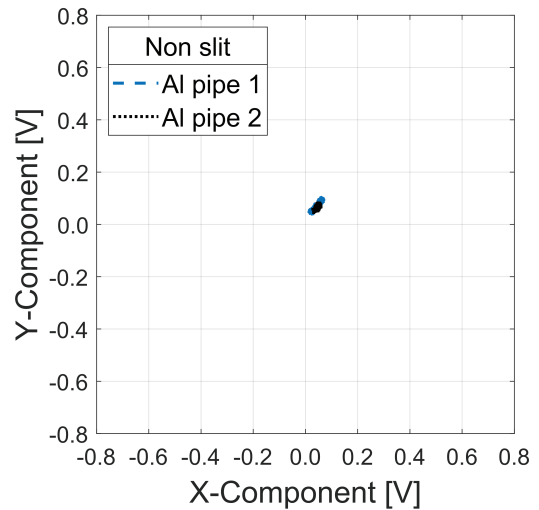
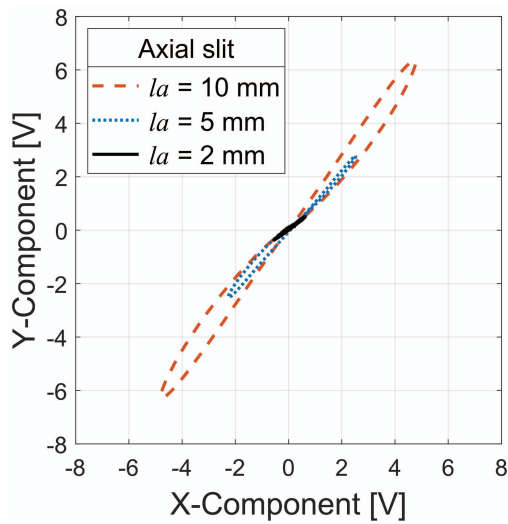
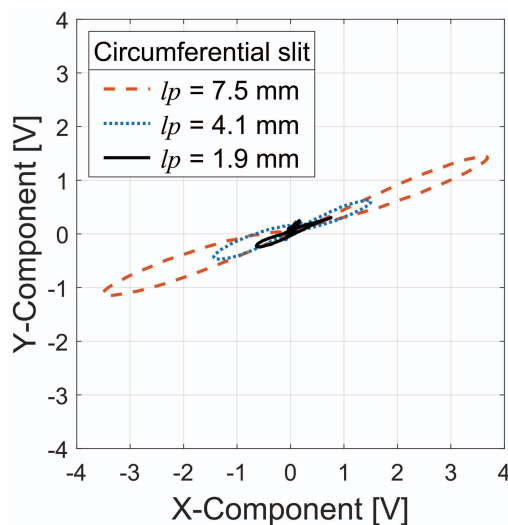


Fig. 7 The trajectories of the ECT signals from aluminum alloy pipes without slits.



(a) Axial penetrated slits



(b) Circumferential penetrated slits

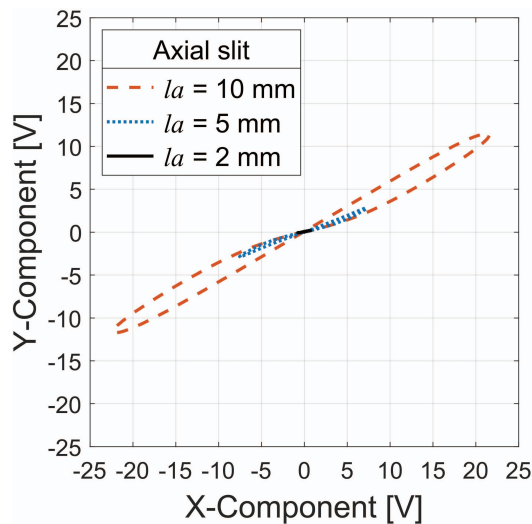
Fig. 6 The trajectories of the ECT signals from the penetrated slits on the F82H pipes.

pipe and affected the magnetism. This should be investigated in the future. In constant, all trajectories shown in Fig. 6 depict an “8” clearly, which indicates that the smallest slits were detectable regardless of their orientations. In addition, the phases of the signals from the axial slits are different from those of the signals from the circumferential ones. This indicates that the signals from the circumferential slits appeared not due to the disturbance of induced eddy currents but due to leaked magnetic fluxes [14].

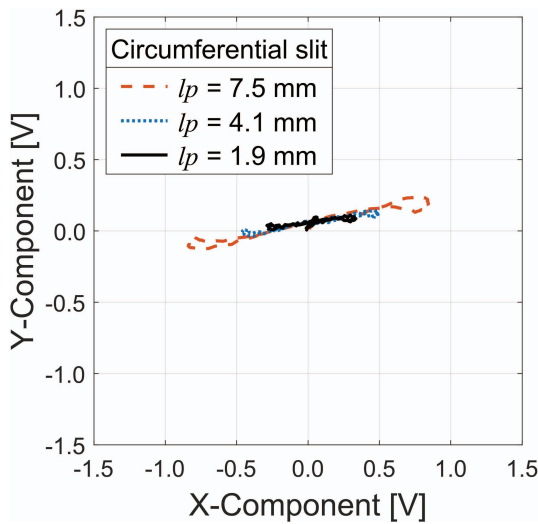
Figures 7 and 8 show the trajectories of the ECT signals from the aluminum alloy pipes without slits and with the penetrated slits, respectively, for comparison. The amplitudes of the two signals due to the pipes without slits, namely noise, shown in Fig. 7 do not differ from each other significantly. In addition, they are much smaller than those in Fig. 5. This is because the aluminum alloy is nonmagnetic, and its electromagnetic property is uniform. Although all the slits were detectable, the amplitudes of the signals from the circumferential slits are much smaller than those from the axial slits. All the trajectories have almost the same phase, which means that all the signals were caused by the disturbance of induced eddy currents unlike the ones shown in Fig. 6. This supports that the physical background of the signals shown in Fig. 6 is due to the leaked magnetic flux from the circumferential slits fabricated in the F82H pipes.

3.1.2 Detectability against the outer surface slits

Figure 9 presents the trajectories of the ECT signals from the F82H pipes with deep outer surface slits. Although the signal from the axial slit with a depth of 0.9 mm is obviously larger than those from the other two slits, its trajectory does not depict an “8” clearly. The signals from the other two outer surface slits are as small as the smallest signal shown in Fig. 5. This indicates that detecting cracks that appear on the outer surface of a pipe is difficult even



(a) Axial penetrated slits



(b) Circumferential penetrated slits

Fig. 8 The trajectories of the ECT signals from the penetrated slits on the aluminum alloy pipes.

when the cracks almost completely penetrate the tube wall. This clearly indicates that a frequency of 100 kHz, which is commonly used to inspect PWR-SGs, is too high to detect flaws on the outer surface of cooling tubes.

3.2 Evaluation of detectability by numerical simulation

3.2.1 Detectability against the inner surface slits

Figure 10 presents the ECT signals from the penetrated slits using an exciting frequency of 100 kHz obtained by the numerical simulations and the calibration. The trajectories shown in Fig. 10 are similar to the ones presented in Fig. 6, which supports the validation of the experiments and the simulations. Figures 11 and 12 compare the peak-to-peak amplitudes of the signals obtained by the experiments and the numerical simulations using an exciting frequency of 100 kHz. The black horizontal lines in the fig-

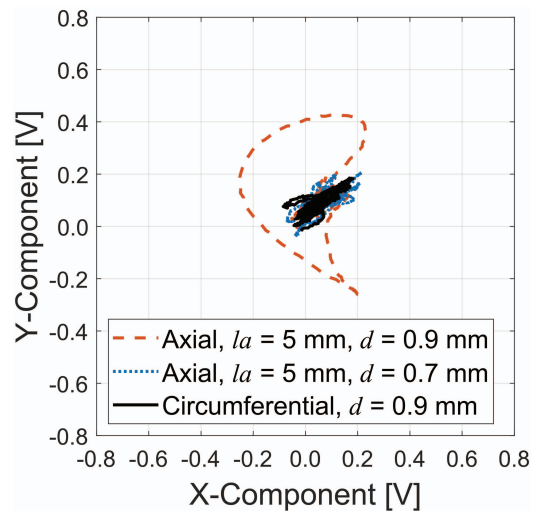
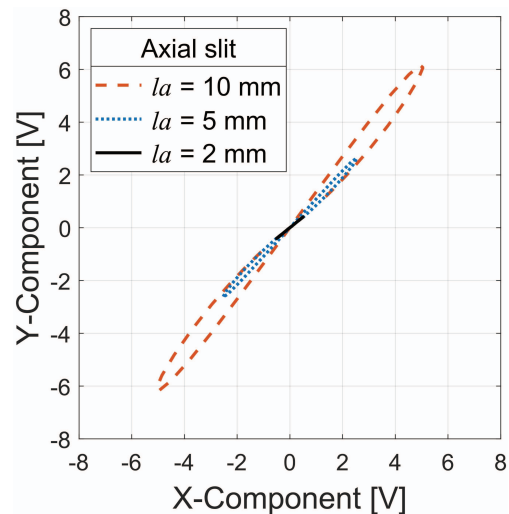
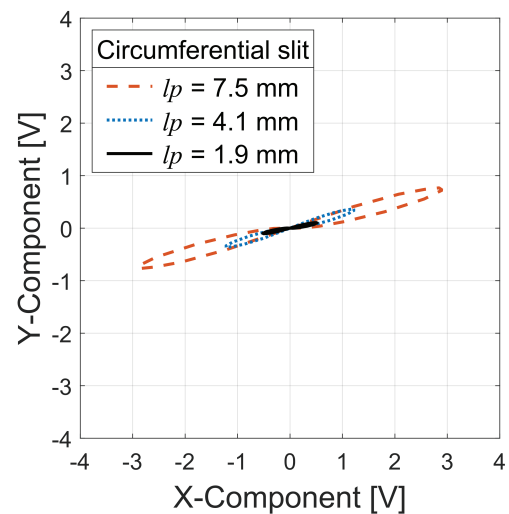


Fig. 9 The trajectories of the ECT signals from the outer surface slits on the F82H pipes.



(a) Axial penetrated slits



(b) Circumferential penetrated slits

Fig. 10 The trajectories of simulation signal from penetrated slits on F82H pipes.

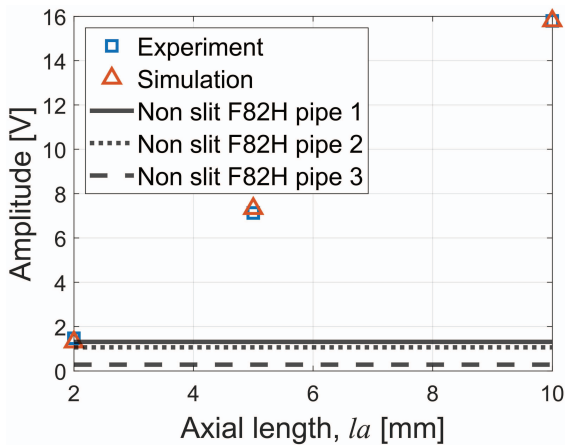


Fig. 11 The amplitudes of the axial penetrated slits.

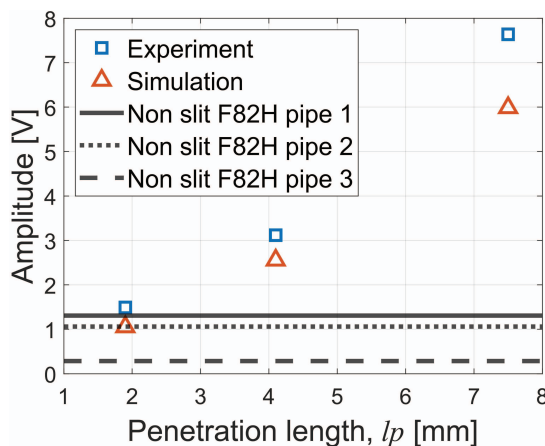


Fig. 12 The amplitudes of the circumferential penetrated slits.

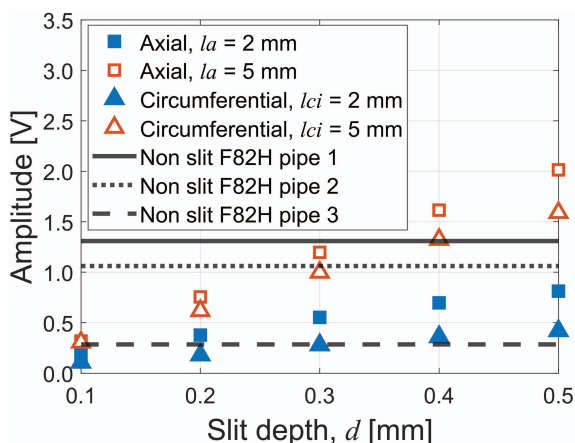


Fig. 13 The amplitudes of inner surface slits on the F82H pipes in the numerical simulation.

ures represent the amplitude of the noise that is evaluated as the lengths of the major axes of the ellipses enveloping the trajectories presented in Fig. 5. Although the signals from the axial slits exhibit good agreement, there is a discrepancy between the experiments and the numerical sim-

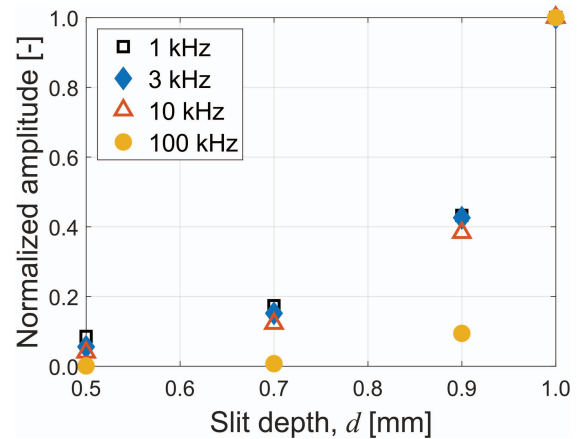


Fig. 14 The amplitudes of the axial outer surface slit with an axial length of 5 mm.

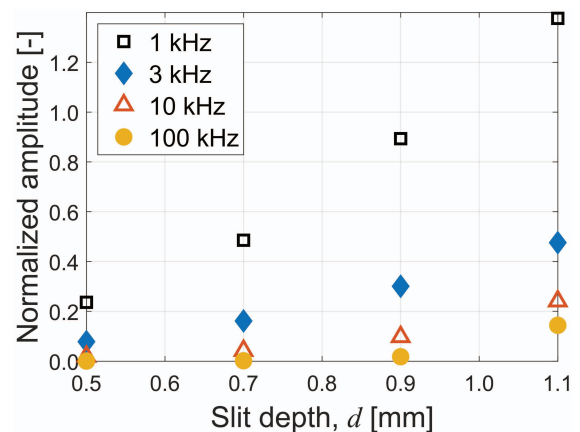


Fig. 15 The amplitudes of the circumferential outer surface slit.

ulations in their signals from the circumferential slits. This is primarily because the signals obtained by the numerical simulations were calibrated using the axial penetrated slit with a length of 10 mm.

Figure 13 summarizes the peak-to-peak amplitudes of the signals from the numerical simulation from the non-penetrating slits on the inner surface of the F82H pipes. The figure supports that the orientation of a slit does not affect the minimum detectable flaw size: approximately 5 mm in length and 0.4 mm in depth. Although it would be possible to improve the detectability by using the phase of signals, the figure indicates that detecting a circumferential slit with a length of 2 mm and depth of 0.3 mm would need improvements of the measurement such as using a probe with a higher spatial resolution and using a higher exciting frequency. The figure implies, however, that detecting a circumferential slit as deep as 0.1 mm would be challenging.

3.2.2 Detectability against the outer surface slits with low exciting frequencies

Figures 14 and 15 summarize the effects of an exciting frequency on the amplitude of the signals from slits on

the outer surface. Note that the outer circumferential slits were modeled as illustrated in Fig. 3 in the numerical simulations. The amplitudes were normalized using the signals from the axial penetrated slit with a length of 5 mm measured at the same exciting frequency, as the amplitude depends on an exciting frequency. The figures indicate that using a low exciting frequency is preferable for detecting non-penetrating circumferential slits. However, exciting frequencies lower than 1 kHz are seldom used in ECT because they lead to a poor signal-to-noise ratio. This would be especially problematic when inspecting a pipe with a small diameter because of the difficulty in using coils with a high number of turns. Other methods such as magnetic saturation or remote field ECT [17–19] would be necessary for the non-destructive inspection of the outer surface.

4. Discussion

A fusion DEMO reactor is in the design stage, and the detailed specification of the cooling tubes has not been decided yet. Consequently, it is difficult to discuss the target detection limit, namely flaws needed to be surely detected, at this stage. In this sense, this study would contribute to the design of cooling tubes. In general, it is necessary to design structures taking consideration of their degradation and how they are non-destructively inspected. This study has confirmed that ECT is applicable to the non-destructive inspection of the cooling tubes, but there are several large differences from ECT applied to the inspection of PWR-SGs so long as the cooling tubes are made of F82H, the first candidate material of the tubes. It is advantageous that a simple bobbin probe is effective in detecting flaws on the inner surface of the tube, whereas the size of the minimum detectable flaw would be somewhat larger than those appearing on the inner surface of PWR-SGs. It is probable that the bobbin probe needs to be driven at two very different frequencies to detect both axial and circumferential flaws. In contrast, however, this study also revealed that ECT would be ineffective in detecting flaws appearing on the outer surface of the cooling tube even though an exciting frequency as low as 1 kHz is adopted. Other methods would be necessary for the non-destructive inspection of the outer surface; it is also important to avoid degradations on the outer surface, rather than those on the inner surface, of the tubes.

5. Conclusion

This study investigated the applicability of ECT to the non-destructive inspecting of the blanket cooling tube of a fusion DEMO reactor. This study considered a specific design of a tube, a pipe made of F82H steel with inner and outer diameters of 9.0 and 11.0 mm, respectively, and

evaluated the applicability of a bobbin probe based on an earlier study by the authors. The results of the experiments and numerical simulations performed in this study revealed that a bobbin probe is effective in detecting cracks on the inner surface of the pipe regardless of whether it is oriented in the axial or circumferential direction because of the magnetic property of F82H steel. In addition, it was demonstrated that the orientation can be distinguished from the signal phase. It is advantageous that a bobbin probe, which has a simple structure, is effective because it indicates that probes with a more complicated structure, such as a plus-point probe and other ones proposed in recent studies [20, 21], would not be required for the non-destructive inspection of the inner surface of the pipe. In contrast, the results of this study confirmed the difficulty in detecting cracks that appear on the outer surface of the pipe. Because the penetration depth depends mainly on the exciting frequency and the properties of the material used, it is plausible that the findings obtained in this study are independent of the size or shape of the cooling tube.

Acknowledgment

This work was supported by QST Research Collaboration for Fusion DEMO.

- [1] S. Tanaka *et al.*, Fusion Eng. Des. **83**, 865 (2008).
- [2] K. Tobita *et al.*, Fusion Sci. Technol. **75**, No. 5, 372 (2019).
- [3] Y. Someya *et al.*, Fusion Eng. Des. **146**, 894 (2019).
- [4] R. Ghoni *et al.*, Adv. Mech. Eng. **6**, 1 (2014).
- [5] H.-S. Shim *et al.*, Nucl. Eng. Des. **197**, 26 (2016).
- [6] H. Huang *et al.*, NDT&E International **36**, 515 (2003).
- [7] H. Tanigawa *et al.*, Fusion Eng. Des. **89**, 1573 (2014).
- [8] H. Sakasegawa *et al.*, Fusion Eng. Des. **98-99**, 2068 (2015).
- [9] T. Nozawa *et al.*, Nucl. Fusion **61**, 116054 (2021).
- [10] G.V. Drunen *et al.*, NDT International **17**, No. 1, 9 (1984).
- [11] M. Kako *et al.*, Proceedings of the 8th Annual Tohoku branch Meeting of Japan Society for Non-Destructive Inspection, 2 (2021).
- [12] M. Kako *et al.*, Proceedings of the 17th Annual Meeting of Japan Society of Maintenance, 403 (2021).
- [13] N. Yusa *et al.*, J. Nucl. Sci. Technol. **51**, 127 (2014).
- [14] H. Hoshikawa *et al.*, Review of Quantitative Nondestructive Evaluation **24**, 494 (2005).
- [15] Nuclear Standards Committee of JEA, Eddy Current Examination for In-service Inspection of Light Water Cooled Nuclear Power Plant Components, JEAG 4208-2012, (2012).
- [16] AC/DC Module User's Guide Version: COMSOL 5.5, COMSOL, Inc.
- [17] A.V. Sukhikh *et al.*, Atomic Energy **102**, No. 2, 139 (2007).
- [18] T.R. Schmidt, Materials Evaluation **42**, No. 2, 225 (1984).
- [19] S.M. Haugland, IEEE Trans. Magn. **32**, No. 4, 3195 (1996).
- [20] N. Lei *et al.*, Int. J. Appl. Electromagn. Mech. **32**, 1279 (2010).
- [21] Q. Yang *et al.*, Sens. Actuators A **331**, 113023 (2021).